

Inhomogeneous chiral condensate in the quark-meson model

Prabal Adhikari,^{1,*} Jens O. Andersen,^{2,†} and Patrick Kneschke^{3,‡}

¹*St. Olaf College, Physics Department, 1520 St. Olaf Avenue, Northfield, MN 55057, USA*

²*Department of Physics, Faculty of Natural Sciences, NTNU,*

Norwegian University of Science and Technology, Høgskoleringen 5, N-7491 Trondheim, Norway

³*Faculty of Science and Technology, University of Stavanger, N-4036 Stavanger, Norway*

(Dated: June 19, 2022)

The two-flavor quark-meson model is used to study inhomogeneous chiral condensates at finite temperature T and baryon chemical potential μ_B . Using a chiral-density wave ansatz for the inhomogeneity, we present the results for the phase diagram of a mean-field calculation of the effective potential. The parameters of the model are determined by matching the meson and quark masses, and the pion constant to their physical values using the on-shell and modified minimal subtraction schemes. In the chiral limit, the size of the inhomogeneous region in the phase diagram depends on whether one includes quantum fluctuations and is also very sensitive to the value of the sigma mass. At the physical point, we find no inhomogeneous phase if one includes quantum corrections.

Introduction

The phase structure of QCD has been subject of interest since its phase diagram was first conjectured in the 1970s. Today, we have a relatively good understanding of the phase transition at zero baryon chemical potential μ_B . At $\mu_B = 0$ one can use lattice simulations and for physical quark masses, the transition is a cross-over at a temperature of around 155 MeV [1–4]. Above the transition temperature QCD is in the quark-gluon plasma phase. At temperatures up to a few times the transition temperature, this is a strongly interacting liquid [5]. For higher temperatures, resummed perturbation theory yields results for the thermodynamic functions that are in good agreement with lattice data [6, 7].

The situation is less clear at finite density and low temperature. Due to the sign problem, this part of the phase diagram is not accessible to standard Monte Carlo techniques based on importance sampling. Only at asymptotically high densities are we confident about the phase and the properties of QCD. In this limit, the ground state of QCD is the color-flavor locked phase which is a color superconducting phase [8]. The color symmetry is completely broken and all the gluons are screened. The low-energy excitations of this phase are Goldstone modes which can be described by a chiral effective Lagrangian. At medium densities, information about the phase diagram has been obtained mainly by using low-energy effective models that share some features with QCD such as chiral symmetry breaking in the vacuum. Examples of low-energy models are the Nambu-Jona-Lasinio (NJL) model and the quark-meson

(QM) model as well as their Polyakov-loop extended versions PNJL and PQM models. At these lower densities, QCD is still in a color-superconducting phase, but the symmetry-breaking pattern is different [8, 9]. The ground state for a given value of the baryon chemical potential is very sensitive to the values of the parameters of the effective models. It turns out that some of the color superconducting phases are inhomogeneous [8–10]. Inhomogeneous phases do not exist only in dense QCD, but also for example in ordinary superconductors and in imbalanced Fermi gases. In the present paper, we reconsider the problem of inhomogeneous chiral-symmetry breaking phases in dense QCD [11, 12] within the QM model. To be specific, we focus on a chiral density wave. The problem of inhomogeneous phases has been addressed before in the context of the Ginzburg-Landau approach [14–17], the NJL [18–22] and PNJL models [23, 24], the QM model [20, 25, 26], and the nonlocal chiral quark model [27]. Most of the work has been done in the mean-field approximation; however, the properties of the Goldstone modes that are associated with the spontaneous symmetry breaking of space-time symmetries are important as they may destabilize the inhomogeneous phase [16, 17]. The destabilization is caused by long-wavelength fluctuations at finite temperature, where long-range order is replaced by algebraic decay of the order parameter. This does not apply at strictly $T = 0$ since the long-wavelength fluctuations are suppressed in this case. Likewise, if the system is in an external magnetic field B , the effect is suppressed [17] and a true condensate can exist also at finite T .

In the next section, we briefly discuss the QM model and explain how we calculate the one-loop effective potential in the large N_c -limit using the on-shell and $\overline{\text{MS}}$ schemes together with dimensional regularization. In Sec. III, we discuss our results and compare them with other calculations.

* adhika1@stolaf.edu

† andersen@tf.phys.ntnu.no

‡ patrick.kneschke@uis.no

Quark-meson model and effective potential

The Euclidean Lagrangian of the two-flavor quark-meson model is

$$\begin{aligned}\mathcal{L} = & \frac{1}{2} [(\partial_\mu \sigma)^2 + (\partial_\mu \boldsymbol{\pi})^2] + \frac{1}{2} m^2 (\sigma^2 + \boldsymbol{\pi}^2) \\ & + \frac{\lambda}{24} (\sigma^2 + \boldsymbol{\pi}^2)^2 - h\sigma \\ & + \bar{\psi}_f [\not{\partial} + \gamma^0 \mu_f - g(\sigma + i\gamma^5 \boldsymbol{\tau} \cdot \boldsymbol{\pi})] \psi_f, \quad (1)\end{aligned}$$

where $f = u, d$ is the flavor index, μ_f is corresponding chemical potential. The quark chemical potential is $\mu = \mu_f = \frac{1}{3}\mu_B$, where μ_B is the baryon chemical potential. In addition to a global $SU(N_c)$ symmetry, the Lagrangian has a $SU(2)_L \times SU(2)_R$ symmetry in the chiral limit, while away from it, the symmetry is reduced to $SU(2)_V$.

In the vacuum, the σ -field acquires a nonzero vacuum expectation value, which we denote by ϕ_0 . In order to study inhomogeneous phases, we must make an ansatz for the space-time dependence of the mesonic mean fields. In the literature, mainly one-dimensional modulations have been considered, for example chiral-density waves (CDW) and soliton lattices. Since the results seem fairly independent of the modulation [25], we opt for the simplest, namely a one-dimensional chiral-density wave. The ansatz is

$$\sigma(z) = \phi_0 \cos(qz), \quad \pi_3(z) = \phi_0 \sin(qz), \quad (2)$$

where ϕ_0 is the magnitude of the wave and q is a wavevector. The mean fields can be combined into a complex order parameter $M(z) = g[\sigma(z) + i\pi_3(z)] = \Delta e^{iqz}$, where $\Delta = g\phi_0$. The dispersion relation of the quarks in the background (2) is known [28]

$$E_\pm^2 = \left(\sqrt{p_\parallel^2 + \Delta^2} \pm \frac{q}{2} \right)^2 + p_\perp^2, \quad (3)$$

where $p_\parallel = p_z$ and $p_\perp^2 = p_x^2 + p_y^2$. In the QCD vacuum, the chiral symmetry is broken by forming pairs of left-handed quarks and right-handed antiquarks (and vice versa). These quark-antiquark pair have zero net momentum and so the chiral condensate is homogeneous with $q = 0$. An inhomogeneous chiral condensate in the vacuum would imply the spontaneous breakdown of rotational symmetry. At finite density, it is possible to form an inhomogeneous condensate by pairing a left-handed quark with a right-handed quark with the same momentum. The net momentum of the pair is nonzero, resulting in an inhomogeneous chiral condensate. A nonzero wavevector q lowers the energy of the

negative branch in (3) and as a result only this branch is occupied by the quarks in this phase [11].

At tree level, the parameters of the Lagrangian (1) m^2 , λ , g^2 , and h are related to the physical quantities m_σ^2 , m_π^2 , m_q , and f_π by

$$m^2 = -\frac{1}{2} (m_\sigma^2 - 3m_\pi^2), \quad \lambda = 3 \frac{(m_\sigma^2 - m_\pi^2)}{f_\pi^2}, \quad (4)$$

$$g^2 = \frac{m_q^2}{f_\pi^2}, \quad h = m_\pi^2 f_\pi. \quad (5)$$

Expressed in terms of physical quantities, the tree-level potential is

$$\begin{aligned}V_{\text{tree}} = & -\frac{1}{4} f_\pi^2 (m_\sigma^2 - 3m_\pi^2) \frac{\Delta^2}{m_q^2} \\ & + \frac{1}{8} f_\pi^2 (m_\sigma^2 - m_\pi^2) \frac{\Delta^4}{m_q^4} - m_\pi^2 f_\pi^2 \frac{\Delta}{m_q}. \quad (6)\end{aligned}$$

The relations in Eqs. (4)–(5) are the parameters determined at tree level and are often used in practical calculations. However, this is inconsistent in calculations that involve loop corrections unless one uses the on-shell (OS) renormalization scheme. In the on-shell scheme, the divergent loop integrals are regularized using dimensional regularization, but the counterterms are chosen differently from the (modified) minimal subtraction ($\overline{\text{MS}}$) scheme. The counterterms in the on-shell scheme are chosen so that they exactly cancel the loop corrections to the self-energies and couplings evaluated on shell, and as a result the renormalized parameters are independent of the renormalization scale and satisfy the tree-level relations (4)–(5). In the $\overline{\text{MS}}$ scheme, the relations (4)–(5) receive radiative corrections and the parameters depend on the renormalization scale. The divergent part of a counterterm in the OS scheme is necessarily the same as the counterterm in the $\overline{\text{MS}}$ scheme. Since the bare parameters are independent of the renormalization scheme, one can write down relations between the renormalized parameters in the $\overline{\text{MS}}$ and the OS scheme. The latter are expressed in terms of the physical masses and couplings in Eqs. (4)–(5) and we can therefore express the renormalized running parameters $m_{\overline{\text{MS}}}^2$, $\lambda_{\overline{\text{MS}}}$, $g_{\overline{\text{MS}}}^2$, and $h_{\overline{\text{MS}}}$ in the $\overline{\text{MS}}$ scheme in terms of the masses m_σ^2 , m_π^2 , and m_q , and the pion decay constant f_π . In Ref. [29], we calculated the parameters in the $\overline{\text{MS}}$ in the chiral limit. We have generalized the results to the physical point. The details of the calculations will be presented elsewhere [30]. The final results for the one-loop effective potential in the large- N_c limit is

$$\begin{aligned}
V_{1\text{-loop}} = & \frac{1}{2} f_\pi^2 q^2 \left\{ 1 - \frac{4m_q^2 N_c}{(4\pi)^2 f_\pi^2} \left[\log \frac{\Delta^2}{m_q^2} + F(m_\pi^2) + m_\pi^2 F'(m_\pi^2) \right] \right\} \frac{\Delta^2}{m_q^2} + \frac{3}{4} m_\pi^2 f_\pi^2 \left\{ 1 - \frac{4m_q^2 N_c}{(4\pi)^2 f_\pi^2} m_\pi^2 F'(m_\pi^2) \right\} \frac{\Delta^2}{m_q^2} \\
& - \frac{1}{4} m_\sigma^2 f_\pi^2 \left\{ 1 + \frac{4m_q^2 N_c}{(4\pi)^2 f_\pi^2} \left[\left(1 - \frac{4m_q^2}{m_\sigma^2} \right) F(m_\sigma^2) + \frac{4m_q^2}{m_\sigma^2} - F(m_\pi^2) - m_\pi^2 F'(m_\pi^2) \right] \right\} \frac{\Delta^2}{m_q^2} \\
& + \frac{1}{8} m_\sigma^2 f_\pi^2 \left\{ 1 - \frac{4m_q^2 N_c}{(4\pi)^2 f_\pi^2} \left[\frac{4m_q^2}{m_\sigma^2} \left(\log \frac{\Delta^2}{m_q^2} - \frac{3}{2} \right) - \left(1 - \frac{4m_q^2}{m_\sigma^2} \right) F(m_\sigma^2) + F(m_\pi^2) + m_\pi^2 F'(m_\pi^2) \right] \right\} \frac{\Delta^4}{m_q^4} \\
& - \frac{1}{8} m_\pi^2 f_\pi^2 \left[1 - \frac{4m_q^2 N_c}{(4\pi)^2 f_\pi^2} m_\pi^2 F'(m_\pi^2) \right] \frac{\Delta^4}{m_q^4} - m_\pi^2 f_\pi^2 \left[1 - \frac{4m_q^2 N_c}{(4\pi)^2 f_\pi^2} m_\pi^2 F'(m_\pi^2) \right] \frac{\Delta}{m_q} \\
& - \frac{N_c q^4}{6(4\pi)^2} + \frac{N_c}{3(4\pi)^2} \left[q \sqrt{\frac{q^2}{4} - \Delta^2} (26\Delta^2 + q^2) - 12\Delta^2 (\Delta^2 + q^2) \log \frac{q + 2\sqrt{\frac{q^2}{4} - \Delta^2}}{2\Delta} \right] \theta\left(\frac{q}{2} - \Delta\right) \\
& - 2N_c T \int_p \left\{ \log \left[1 + e^{-\beta(E_\pm - \mu)} \right] + \log \left[1 + e^{-\beta(E_\pm + \mu)} \right] \right\}, \tag{7}
\end{aligned}$$

where E_\pm is given by Eq. (3) and a sum over \pm is implied. Moreover, $F(p^2) = 2 - 2\text{Re}[r \arctan(\frac{1}{r})]$, with $r = \sqrt{\frac{4m_q^2}{p^2} - 1}$. We note that the vacuum part of the effective potential (obtained by setting $q = \mu = T = 0$) of Eq. (7) has its minimum at $\Delta = m_q$ by construction, as does the tree-level potential Eq. (6). The result for the vacuum part of the effective potential is completely analytic and obtained using dimensional regularization. At $T = 0$, the matter part of the potential can also be calculated analytically.

In the chiral limit, one can perform a Ginzburg-Landau analysis in order to locate the position of the tricritical point (CP) and the Lifschitz point (LP). The CP is given by the condition that the coefficients of the quadratic and quartic terms vanish. The LP is given by the condition that the coefficients of the quadratic and gradient terms vanish. The result for the CP is

$$0 = -\frac{1}{4} \frac{m_\sigma^2 f_\pi^2}{m_q^2} \left\{ 1 + \frac{4N_c m_q^2}{(4\pi)^2 f_\pi^2} \left[\left(1 - \frac{4m_q^2}{m_\sigma^2} \right) F(m_\sigma^2) \right] + \frac{4m_q^2}{m_\sigma^2} \right\} + N_c \left[\frac{T^2}{6} + \frac{\mu^2}{2\pi^2} \right], \tag{8}$$

$$0 = \frac{1}{8} \frac{m_\sigma^2 f_\pi^2}{m_q^4} \left\{ 1 + \frac{4N_c m_q^2}{(4\pi)^2 f_\pi^2} \left[4 \frac{m_q^2}{m_\sigma^2} \left(\log \frac{m_q^2}{4T^2} + 2\gamma_E + 2\text{Li}'_{-2\epsilon_{\text{IR}}}(-e^{-\beta\mu}) + 2\text{Li}'_{-2\epsilon_{\text{IR}}}(-e^{\beta\mu}) \right) + \left(1 - \frac{4m_q^2}{m_\sigma^2} \right) F(m_\sigma^2) \right] \right\}, \tag{9}$$

where $\text{Li}'_a(x) = \frac{\partial \text{Li}_a(x)}{\partial a}|_{a=0}$, and $\text{Li}_a(x)$ is a polylogarithmic function. The subscript IR indicates that we have used dimensional regularization to regulate infrared divergences that appear in the calculation of Eq. (9) but cancel in the end. The result for the LP is given by Eq. (8) and

$$\frac{1}{2} \frac{f_\pi^2}{m_q^2} \left\{ 1 + \frac{4N_c m_q^2}{(4\pi)^2 f_\pi^2} \left[\log \frac{m_q^2}{4T^2} + 2\gamma_E + 2\text{Li}'_{-2\epsilon_{\text{IR}}}(-e^{-\beta\mu}) + 2\text{Li}'_{-2\epsilon_{\text{IR}}}(-e^{\beta\mu}) \right] \right\} = 0. \tag{10}$$

We notice that for the special case $m_\sigma = 2m_q$, the CP and LP coincide, which happens to be the relation between the sigma and quark masses in the NJL model [31]. In the chiral limit, this also implies that $\lambda = 12g^2$, cf. Eqs. (4)–(5). This relation also holds at the one-loop level at large N_c [25, 30].

Results and discussion

In the numerical work, we set $N_c = 3$ everywhere. We use a constituent quark mass $m_q = 300$ MeV. Since the sigma mass is not very well known experimentally [32], we allow it to vary around $m_\sigma = 600$ MeV. At the physical point we take $m_\pi = 140$ MeV and for the pion

decay constant we use $f_\pi = 93$ MeV.

It is known from earlier studies in the homogeneous case that vacuum fluctuations play an important role. If we omit the quantum fluctuations, the phase transition in the chiral limit is first order in the entire μ - T plane. If they are included the transition is first order for $T = 0$

and second order for $\mu = 0$. The first-order line starting on the μ -axis ends at a tricritical point.

In the inhomogeneous case, we therefore examine the importance of these fluctuations as well. In Fig. 1, we show the phase diagram in the μ - T plane in the chiral limit without vacuum fluctuations. The solid lines indicate a first-order transition while the dashed line indicates a second-order transition. The region between the two red lines is the inhomogeneous phase. The black line is the first-order transition line in the homogeneous case.

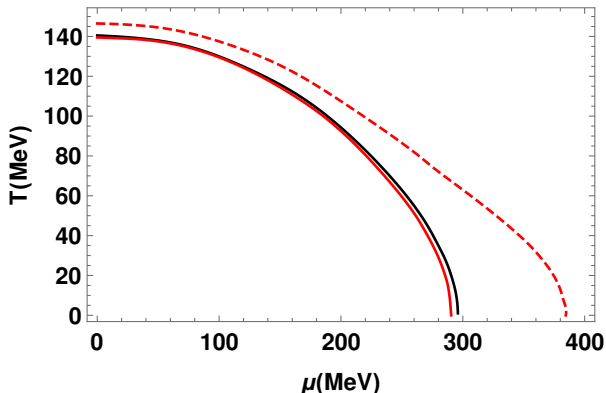


FIG. 1. The phase diagram in the μ - T plane for $m_q = 300$ MeV and $m_\sigma = 600$ MeV in the chiral limit without quantum fluctuations. A dashed line indicates a second-order transition, while a solid line indicates a first-order transition. The region between the red lines is the inhomogeneous phase.

In Fig. 2, we show the phase diagram in the μ - T plane in the chiral limit where vacuum fluctuations are included. The inhomogeneous phase in the entire μ - T plane has now been replaced by a small region at low temperatures. The second-order line starting at $\mu = 0$ end at the Lifschitz point indicated by the full red circle. Its coordinates are $(303, 55)$. Since $m_\sigma = 2m_q$ this is also the position of the tricritical point. In all cases there is agreement between the numerical calculation of the coordinates of the CP and LP and their coordinates obtained by solving Eqs. (8)–(10). The region between the two red lines is the inhomogeneous phase. Comparing Figs. 1 and 2, we see the dramatic effects of including the fermionic vacuum fluctuations.

In Fig. 3, we show the modulus Δ (blue line) and the wavevector q (red line) as functions of μ at $T = 0$ in the chiral limit with $m_\sigma = 2m_q = 600$ MeV. The transition from a phase with homogeneous condensate to a phase with a chiral density wave is first order, while the transition to a chirally symmetric phase is second order.

In Fig. 4, we show the phase diagram in the μ - T plane in the chiral limit where vacuum fluctuations are

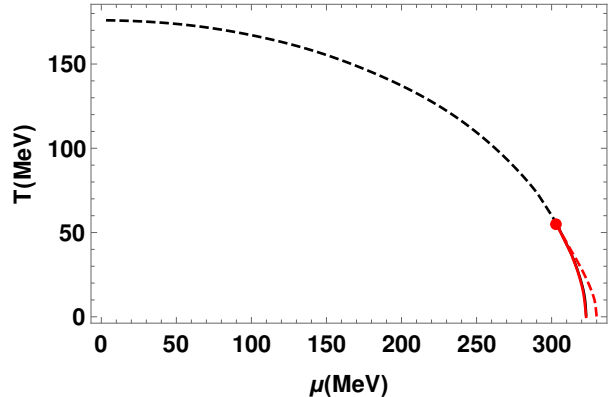


FIG. 2. The phase diagram in the μ - T plane for $m_q = 300$ MeV and $m_\sigma = 600$ MeV in the chiral limit including vacuum fluctuations. A dashed line indicates a second-order transition, while a solid line indicates a first-order transition. The region between the red lines is the inhomogeneous phase.

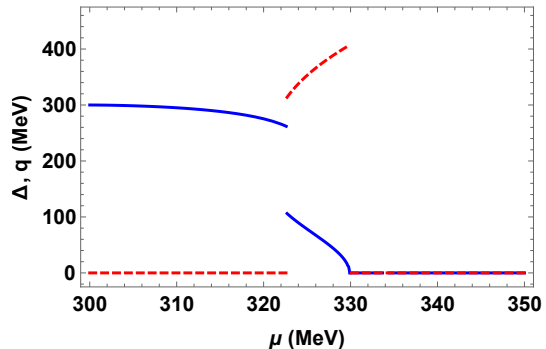


FIG. 3. (Color online) Gap Δ (blue line) and wavevector q (red line) as functions of the quark chemical potential μ in the chiral limit, at $T = 0$, and for $m_\sigma = 2m_q = 600$ MeV.

included. The sigma mass is $m_\sigma = 620$ MeV. A dashed line indicates a second-order transition, while a solid line indicates a first-order transition. The full red circle indicates the LP while the full black circle indicates the CP. Their positions are $(325, 42)$ and $(311, 66)$. The black solid line is the first-order transition line in the homogeneous case. The region of the inhomogeneous phase is significantly larger than in Fig. 2 where $m_\sigma = 600$ MeV. The size of the inhomogeneous phase depends sensitively on the value of the sigma mass and disappears for $m_\sigma \lesssim 590$ MeV.

Our results in the chiral limit are in good agreement with those obtained in Ref. [25], where the authors use Pauli-Villars regularization to calculate the parameters of the model and the effective potential itself. They also investigate another modulation, namely a soliton lattice.

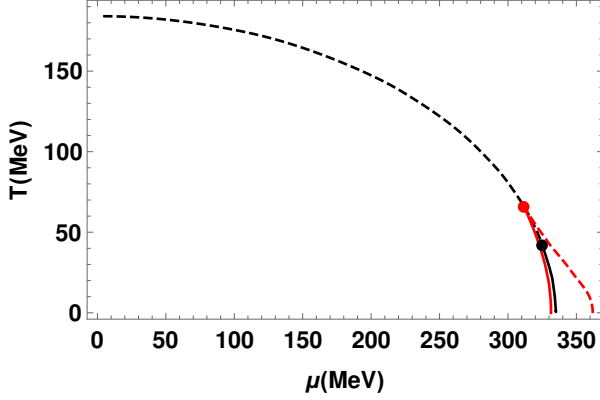


FIG. 4. The phase diagram in the μ - T plane for $m_q = 300$ MeV and $m_\sigma = 620$ MeV in the chiral limit including vacuum fluctuations. A dashed line indicates a second-order transition, while a solid line indicates a first-order transition. The region between the red lines is the inhomogeneous phase.

The region in the phase diagram with an inhomogeneous phase is slightly larger than for a chiral density wave and it is also favored over the latter.

We next consider the physical point. In Fig. 5, we show the phase diagram in the μ - T plane at the physical point omitting quantum corrections. The transition from the phase with a homogeneous condensate to a phase with an inhomogeneous condensate is first order for all T . The solid line is the first-order transition in the homogeneous case ending in a tricritical point whose coordinates are (221.5, 92). The green line indicates the crossover extending to $\mu = 0$.

The behavior is very different if we include quantum corrections. Here it turns out that there is no inhomogeneous phase, but a crossover in the entire μ - T plane from a chirally broken phase to a phase where chiral symmetry is approximately restored. We therefore do not show the phase diagram itself, but focus on the behavior of the order parameter. In Fig. 6, we show the gap Δ as a function of μ for three different temperatures. The results are without vacuum fluctuations. For $T = 0$ and $T = 50$ MeV, the transition is clearly first order, while for $T = 100$ MeV, it is a crossover.

In Fig. 7, we show the gap Δ as a function of μ for three different temperatures. The results are obtained including vacuum fluctuations. For all temperatures, the transition is a crossover. We have calculated the largest value of m_π for which there is an inhomogeneous phase and found the critical value $m_\pi^c = 92$ MeV. Similar results were found in Ref. [20] in the context of the NJL model and a soliton lattice; the region of the inhomogeneous phase shrinks as one increases the pion mass. However, at the physical point, a small inhomogeneous region still exists and the transition from the phase with

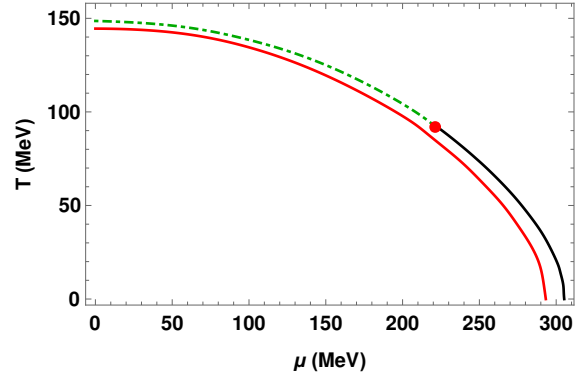


FIG. 5. The phase diagram in the μ - T plane for $m_q = 300$ MeV and $m_\sigma = 600$ MeV at the physical point and without quantum fluctuations. A dashed line indicates a crossover transition, while a solid line indicates a first-order transition. Below the red line, the condensate is homogenous and above it, the condensate is inhomogeneous. The full red circle denotes the critical endpoint.

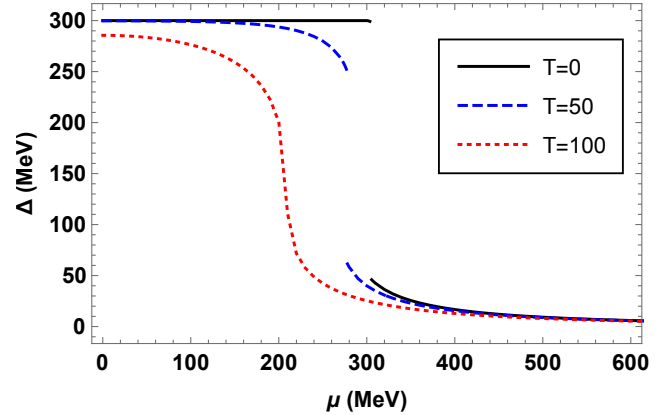


FIG. 6. Gap Δ for three different temperatures with $m_\sigma = 600$ MeV and $m_\pi = 140$ MeV without vacuum fluctuations.

a homogeneous chiral condensate to the phase with an inhomogeneous chiral condensate as well as the transition to the chirally symmetric phase are first order.

To summarize, we have studied inhomogeneous phases using the QM model as an effective low-energy model for QCD assuming a chiral density wave. Our results do not exclude inhomogeneous phases in general but suggest that their existence is very sensitive to the sigma and pion masses.

In Ref. [17], it is shown that the Goldstone bosons that arise from the breaking of the translational and rotational symmetry have a quadratic dispersion relation in some directions. At finite temperature, this leads

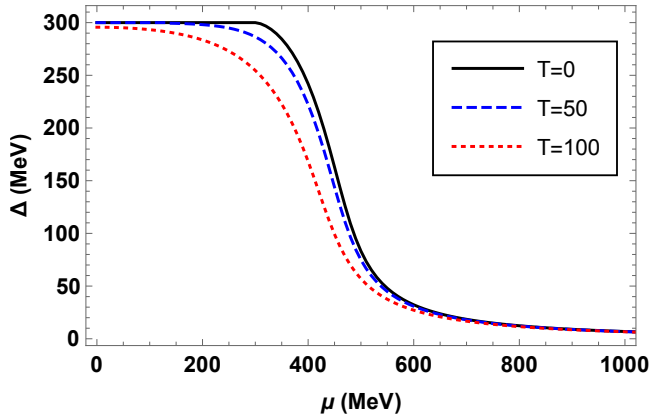


FIG. 7. Gap Δ for three different temperatures with $m_\sigma = 600$ MeV and $m_\pi = 140$ MeV with vacuum fluctuations.

to strong long wavelength fluctuations that destroy off-diagonal long-range order altogether. Long-range order is replaced by quasi-long-range order where the order pa-

rameter is decaying algebraically. At $T = 0$, the phase fluctuations are not strong enough to destroy this order and there is a true condensate. In a constant magnetic background, they also showed that the dispersion relation is linear in all directions. This implies that the infrared divergences that signal the instability of long-range order are absent and that an inhomogeneous phase with a constant magnitude can exist even at finite temperature.

ACKNOWLEDGMENTS

The authors would like to thank S. Carignano for useful discussions. P.A. would like to acknowledge the research travel support provided through the Professional Development Grant and would like to thank the Faculty Life Committee and the Dean's Office at St. Olaf College. P.A. would also like to acknowledge the computational support provided through the Computer Science Department at St. Olaf College and thank Richard Brown, Tony Skalski and Jacob Caswell. P. A. and P. K. would like to thank the Department of Physics at NTNU for kind hospitality during the latter stages of this work.

-
- [1] Y. Aoki, Z. Fodor, S. Katz, and K. Szabo, Phys. Lett. B **643**, 46 (2006),
 - [2] Y. Aoki, S. Borsanyi, S. Durr, Z. Fodor, S.D. Katz et al., JHEP **0906**, 088 (2009),
 - [3] S. Borsanyi et al. (Wuppertal-Budapest Collaboration), JHEP **1009**, 073 (2010)
 - [4] A. Bazavov, T. Bhattacharya, M. Cheng, C. DeTar, H. Ding et al., Phys.Rev. D **85**, 054503 (2012).
 - [5] J. Casalderrey-Solana, H. Liu, D. Mateos, K. Rajagopal, and U. A. Wiedemann, Gauge/String Duality, Hot QCD and Heavy Ion Collisions. Cambridge University Press, (2014).
 - [6] S. Mogliacci, J. O. Andersen, M. Strickland, N. Su, A. Vuorinen, JHEP **1312**, 055 (2013).
 - [7] N. Haque, A. Bandyopadhyay, J. O. Andersen, M. G. Mustafa, M. Strickland, and N. Su, JHEP **1405**, 027 (2014).
 - [8] M. G. Alford, A. Schmitt, and K. Rajagopal, Rev. Mod. Phys. **80**, 1455 (2008),
 - [9] K. Fukushima, and T. Hatsuda, Rept. Prog. Phys. **74**, 014001 (2011).
 - [10] R. Anglani, R. Casalbuoni, M. Ciminale, N. Ippolito, R. Gatto, M. Mannarelli, and M. Ruggieri, Rev. Mod. Phys. **86**, 509 (2014).
 - [11] M. Buballa and S. Carignano, Prog. Part. Nucl. Phys. **81**, 39 (2015).
 - [12] T. Kojo, Y. Hidaka, L. McLerran, and R. D. Pisarski, Nucl. Phys. A **843**, 37 (2010); *ibid* **875**, 94, (2011).
 - [13] K. Fukushima, Phys. Rev. D **78**, 114019 (2008).
 - [14] D. Nickel, Phys. Rev. Lett. **103**, 072301 (2009).
 - [15] H. Abuki and D. Ishibashi, Phys. Rev. D **85**, 074002 (2012).
 - [16] T.-G. Lee, E. Nakano, Y. Tsue, T. Tatsumi, B. Friman, Phys. Rev. D **92**, 034024 (2015).
 - [17] Y. Hidaka, K. Kamikado, T. Kanazawa, and T. Noumi, Phys. Rev. D **92**, 034003 (2015).
 - [18] E. Nakano and T. Tatsumi, Phys. Rev. D **71**, 114006 (2005).
 - [19] S. Maedan, Prog. Theor. Phys. **123**, 285 (2010).
 - [20] D. Nickel, Phys. Rev. D **80**, 074025 (2009).
 - [21] S. Karasawa and T. Tatsumi, Phys. Rev. D **92**, 116004 (2015).
 - [22] A. Heinz, F. Giacosa, M. Wagner, and D. H. Rischke, Phys. Rev. D **93**, 014007 (2016)
 - [23] S. Carignano, D. Nickel, and M. Buballa, Phys. Rev. D **82**, 054009 (2010).
 - [24] J. Braun, F. Karbstein, S. Rechenberger, and D. Roscher Phys. Rev. D **93**, 014032 (2016).
 - [25] S. Carignano, M. Buballa, and B.-J. Schaefer, Phys. Rev. D **90**, 014033 (2014).
 - [26] S. Carignano, M. Buballa, and W. El-Kamhaw, Phys. Rev. D **94**, 034023 (2016).
 - [27] J. P. Carlomagno, D. Gomez Dumm, and N. N. Scoccola, Phys. Rev. D **92**, 056007 (2015).
 - [28] F. Dautry and E. M. Nyman, Nucl. Phys. A **319**, 323 (1979).
 - [29] P. Adhikari, J. O. Andersen, and Patrick Kneschke, e-Print: arXiv:1612.03668 [hep-ph].

- [30] P. Adhikari, J. O. Andersen, and Patrick Kneschke, in preparation.
- [31] S. Klevansky, Rev. Mod. Phys. **64**, 649 (1992).
- [32] Particle data group, <http://pdg.lbl.gov/2014/listings/rpp2014-list-f0-500.pdf>.